Advanced Composites and Hybrid Materials (2023) 6:39
https://doi.org/10.1007/s42114-022-00619-8

RESEARCH

Carbon dots: building a robust optical shield for wood preservation

Youqi Han[1] · Yuning Wang[1] · Bin Zhao[1] · Yibing Bai[1] · Shiyan Han[1] · Yahui Zhang[2] · Shujun Li[1] · Zhijun Chen[1] · Chuanling Si[3] · Haipeng Yu[1] · Chunlei Zhang[1] · Wenji Yu[2]

Received: 19 October 2022 / Revised: 27 December 2022 / Accepted: 28 December 2022 / Published online: 11 January 2023

Abstract
Wood is a sustainable building material that can help to achieve carbon neutralization but, because wood is easily damaged by ultraviolet (UV) light, it is important to protect wood from this harmful radiation. Here, we synthesized sustainable biomass-based carbon dots (Bio-CDs) using only microcrystalline cellulose, which was concentration-dependent and capable of absorbing short wavelength and converting it to long wavelength light emission. Furthermore, the Bio-CDs were mixed with poly (vinyl alcohol) (PVA) to produce robust optical shielding films (OSFs). The results showed that OSFs had good optical properties, which could effectively block UV and high-energy blue photons radiation by absorbing short wavelength light and converting it into longer wavelength (> 450 nm) light. The extent of UV and high-energy blue photons blocking can be easily adjusted by varying the proportion of Bio-CDs in the film. The OSFs have good optical properties and have been successfully used to protect wood from UV damage. This study, which uses environmentally friendly and simple methodology, provides an example of sustainable research.

Keywords Cellulose · Biomass-based carbon dots (Bio-CDs) · Concentration-dependent emission · Optical shielding film (OSF) · Wood protection

1 Introduction

Wood is an important sustainable building material that has a key role in achieving carbon neutralization [1–3]. Because of its good mechanical strength and attractive texture, wood is highly prized for both outdoor construction projects and interior decoration [4–7]. One downside of wood, however, is that long-term exposure to the short wavelength radiation in sunlight leads to degradation of lignin, the main component of wood [8, 9]. This leads to changes in the surface color of the wood and loss of mechanical strength, which affects the processing and use of wood products. Current, several materials including inorganic nanoparticles and organic materials have been developed to protect wood from damaging ultraviolet (UV) irradiation [10–12]. These substances usually fill the interior spaces between wood fibers or form coatings on the surface and are difficult to remove [11, 12]. Available protective materials are also limited by lack of sustainability and high cost of preparation, which means that there is a real need for new, sustainable, inexpensive, and easily prepared UV-blocking materials to protect wood from damaging UV irradiation [12, 13]. Therefore, it is particularly important to find protective materials that can directly block UV rays.

Carbon dots (CDs) are a new type of zero-dimensional nanomaterial. Compared with traditional photoluminescent materials, such as rare earth elements and semiconductor quantum dots, CDs have the advantages of easy preparation, abundant raw materials, low price, tunable emission, optical stability, and good biocompatibility, thus represent a new generation of photoluminescent materials with light absorption and conversion properties [14, 15]. Among many raw materials that can be used for the preparation of CDs, biomass

Youqi Han and Yuning Wang contributed equally to this work.

✉ Shiyan Han
hanshiyan80@163.com

✉ Chuanling Si
sichli@tust.edu.cn

✉ Wenji Yu
yuwenji@caf.ac.cn

[1] Engineering Research Center of Advanced Wooden Materials (Northeast Forestry University), Ministry of Education, Harbin 150040, China

[2] Research Institute of Wood Industry, Chinese Academy of Forestry, Beijing 100091, China

[3] Tianjin Key Laboratory of Pulp and Paper, Tianjin University of Science and Technology, Tianjin 300457, China

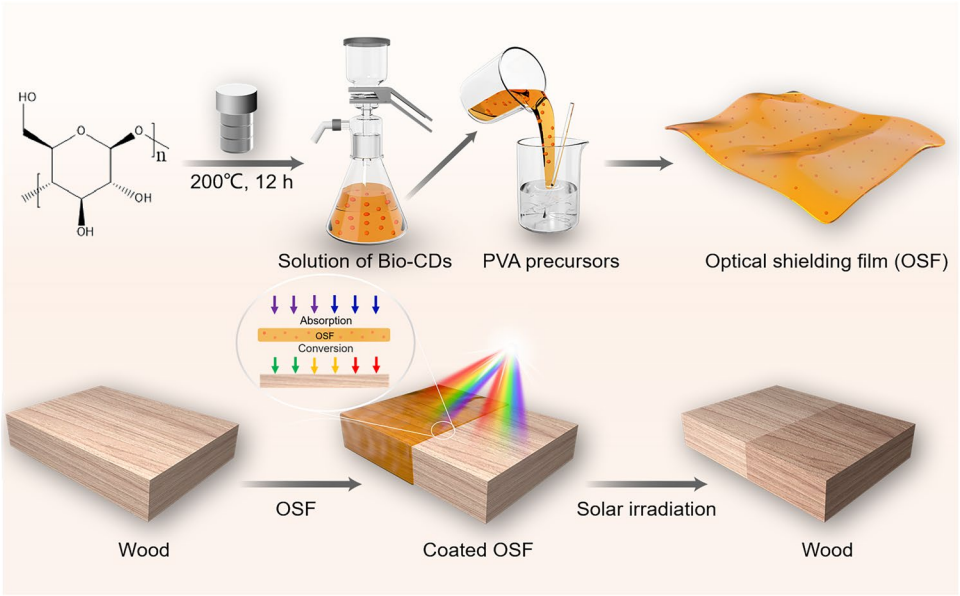

Scheme 1 Schematic showing formation of OSF and its use as a protective coating for wood

is particularly attractive because of its abundant sources, low price, green environmental, and sustainability [16–19]. Among them, cellulose is an abundant biomass resource that has been widely studied and used because it is environmentally friendly and highly sustainable [20–24]. With the extensive research of biomass carbon dots [16], cellulose has also become one of the sustainable carbon sources [5, 25].

In this work, biomass-based CDs (Bio-CDs) were synthesized by one-step hydrothermal method, with microcrystalline cellulose as the raw material and deionized water as the solvent. Aqueous solutions of the Bio-CDs show concentration-dependent optimum excitation and maximum emission tunable properties. As the concentration of Bio-CDs increases, so does the ability of the Bio-CDs to absorb short wavelength light and convert it into long wavelength light emission. This showed that the Bio-CDs could absorb UV and high-energy blue photons to convert them into long wavelength emission. The Bio-CDs thus can be used as UV and high-energy blue photons blocking units, which can be mixed with polyvinyl alcohol (PVA) to prepare optical shielding films (OSFs) (Scheme 1). As expected from the optical properties of the Bio-CDs in solution, the OSFs can absorb short wavelength and convert it into long wavelength emission. Covering the surface of wood with OSF provides good protection from UV and high-energy blue photons while maintaining the texture and surface color of the wood (Scheme 1). No organic solvents are used in the preparation of the OSFs and the whole process is not only green and environmentally friendly, but also conforms to the concept of carbon neutralization. This study provides an example of sustainable research and illustrates the potential of biomass-derived Bio-CDs for blocking UV and high-energy blue photons.

2 Experimental section

2.1 Synthesis of Bio-CDs

The Bio-CDs were synthesized using a hydrothermal approach. Microcrystalline cellulose (0.2 g) was placed in a 100-mL teflon-lined autoclave, and deionized water (70 mL) was added. The mixture was stirred thoroughly for 10 min using a glass rod until the microcrystalline cellulose was completely dispersed. The solution was then heated to 200 °C for 12 h. After cooling naturally to room temperature, the solution was filtered through a 0.22-μm micro-filtration membrane to remove insoluble matter and the filtrate was freeze-dried to provide a sticky solid. The viscous solid was redissolved in deionized water and filtered through a 0.22-μm micro-filtration membrane to remove further insoluble matter. The filtrate was allowed to stand at room temperature for 3 days and then filtered through a 0.22-μm micro-filtration membrane to remove the precipitate. The filtrate was freeze-dried to provide Bio-CDs.

2.2 Preparation of optical shielding films (OSFs)

Add an appropriate amount of Bio-CDs aqueous solution (5 mg/mL) to a mixture of PVA (1 g) and deionized water (25 mL) in a glass beaker. The solutions were stirred in a constant temperature water bath at 95℃ for 1 h and then ultrasonicated for 1 h. Then, cool naturally to room temperature, pour the mixed solution into the square petri dishes (5 cm × 5 cm) and dried at room temperature to form eight different optical shielding films (OSFs), containing 0, 4.5, 6, 7.5, 9, 10.5, 20, or 30% Bio-CDs, respectively.

2.3 Measurement of wood surface color

The surface color of wood is obtained by averaging value of testing three times with NR110 precision colorimeter (Suzhou Tianyuli Instrument Co., Ltd., Suzhou, China), according to the L^*, a^*, and b^* color system set out in the Commission Internationale de l'Eclairage (CIE) Proceedings (1931). The color difference value (ΔE) was calculated using the following formula (1):

$$\Delta E = \sqrt{\Delta L *^2 + \Delta a *^2 + \Delta b *^2} \quad (1)$$

where ΔL^*, Δa^*, and Δb^* are the total changes of L^*, a^*, and b^* values, after illumination, respectively.

3 Results and discussion

Observation of the microscopic morphology of the Bio-CDs by TEM showed small particles with good dispersion (Fig. 1a), no lattice and an average particle size of 7.83 nm (Fig. 1b). AFM analysis was essentially consistent with the TEM analysis and confirmed that the Bio-CDs were small spherical particles (Fig. S1). The XRD pattern of the Bio-CDs showed an obvious diffraction peak at 20.35° (Fig. 1c), corresponding to the (002) plane of graphitic carbon [25, 26]. Raman spectroscopy showed that the Bio-CDs had a mainly a disordered D band (1351 cm^{-1}) and an ordered G band (1590 cm^{-1}) [27, 28] (Fig. 1d), and the I_G/I_D was 0.97, indicating that the Bio-CDs have a graphite-like structure [29, 30].

We also investigated the structure of the Bio-CDs by X-ray photoelectron spectroscopy (XPS) and FT-IR spectroscopy. XPS showed that the Bio-CDs contained the elements C (70.7%) and O (29.3%) (Fig. 2a). The high-resolution C 1 s spectrum showed three peaks at 284.5 eV, 285.8 eV and 287.8 eV, corresponding to C–C/C = C, C-O, and C = O bonds [31–33], respectively (Fig. 2b). The O 1 s spectrum showed two peaks at 530.7 eV and 532.1 eV, corresponding to C = O [34] and C-O bonds [34, 35], respectively (Fig. 2c). The FT-IR spectrum of the Bio-CDs showed characteristic absorption peaks corresponding to – OH groups (3300 cm^{-1}) [36, 37], $-CH_3/-CH_2$ groups (2875–2930 cm^{-1}) [36, 38], C = O groups (1665 cm^{-1}) [39, 40], aromatic rings (1600 cm^{-1}, 1516 cm^{-1}, 1450 cm^{-1}) [41, 42], and C-O groups (1192 cm^{-1}) [41] (Fig. 2d), confirmed the presence of abundant functional groups on the surface of the carbon cores. The existence of these groups may cause diversification of the surface states of Bio-CDs [25], thus increasing the capacity of the Bio-CDs to absorb short wavelength light [25, 26].

Having determined the structure of the Bio-CDs, we next investigated their optical properties. The UV absorption spectrum showed two absorption peaks at 226 nm and 282 nm (Fig. 3a), which were attributed to the π-π* transition of C = C bonds and the *n*-π* transition of C = O bonds, respectively [27, 42, 43]. The absorbance of Bio-CDs aqueous solution intensified and extended to longer wavelengths as their concentration increased (Fig. 3a), demonstrating that Bio-CDs have adjustable capacity for optical absorption in the UV to blue light region. Solutions of Bio-CDs with different concentrations all showed excitation wavelength dependence (Fig. S2), and the excitation spectra of Bio-CDs solutions were consistent with the results of the emission spectra (Fig. S3). We further showed that the

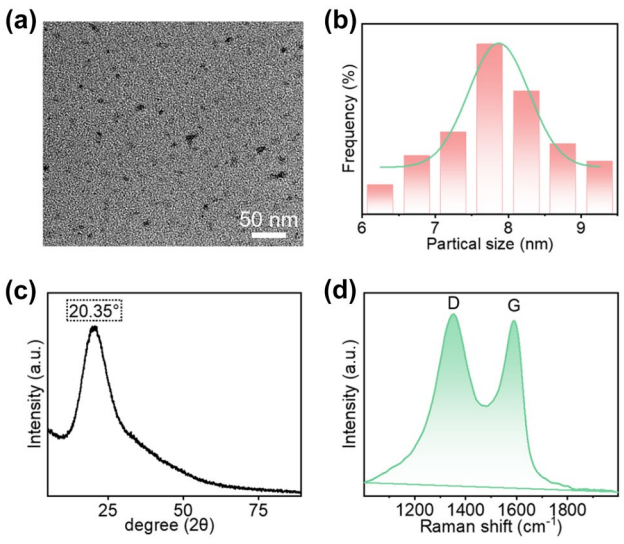

Fig. 1 **a** TEM image of Bio-CDs; **b** particle size histogram of Bio-CDs; **c** XRD spectrum of Bio-CDs; **d** Raman spectrum of Bio-CDs

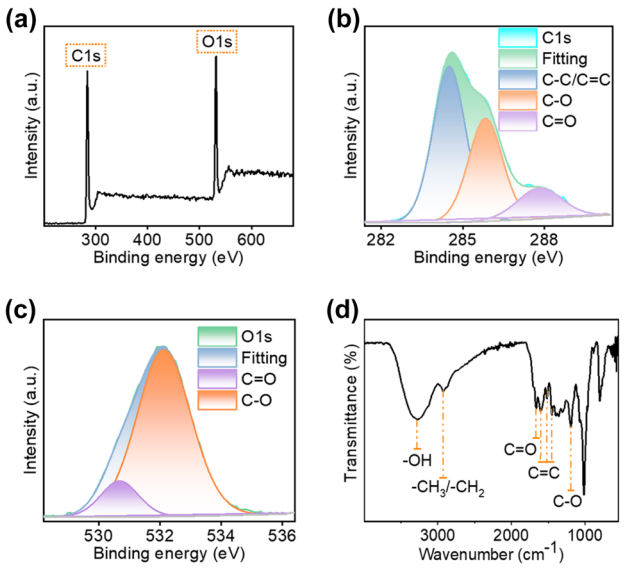

Fig. 2 **a** XPS spectrum of Bio-CDs; **b** C1s XPS spectrum of Bio-CDs; **c** O1s XPS spectrum of Bio-CDs; **d** FT-IR spectrum of Bio-CDs

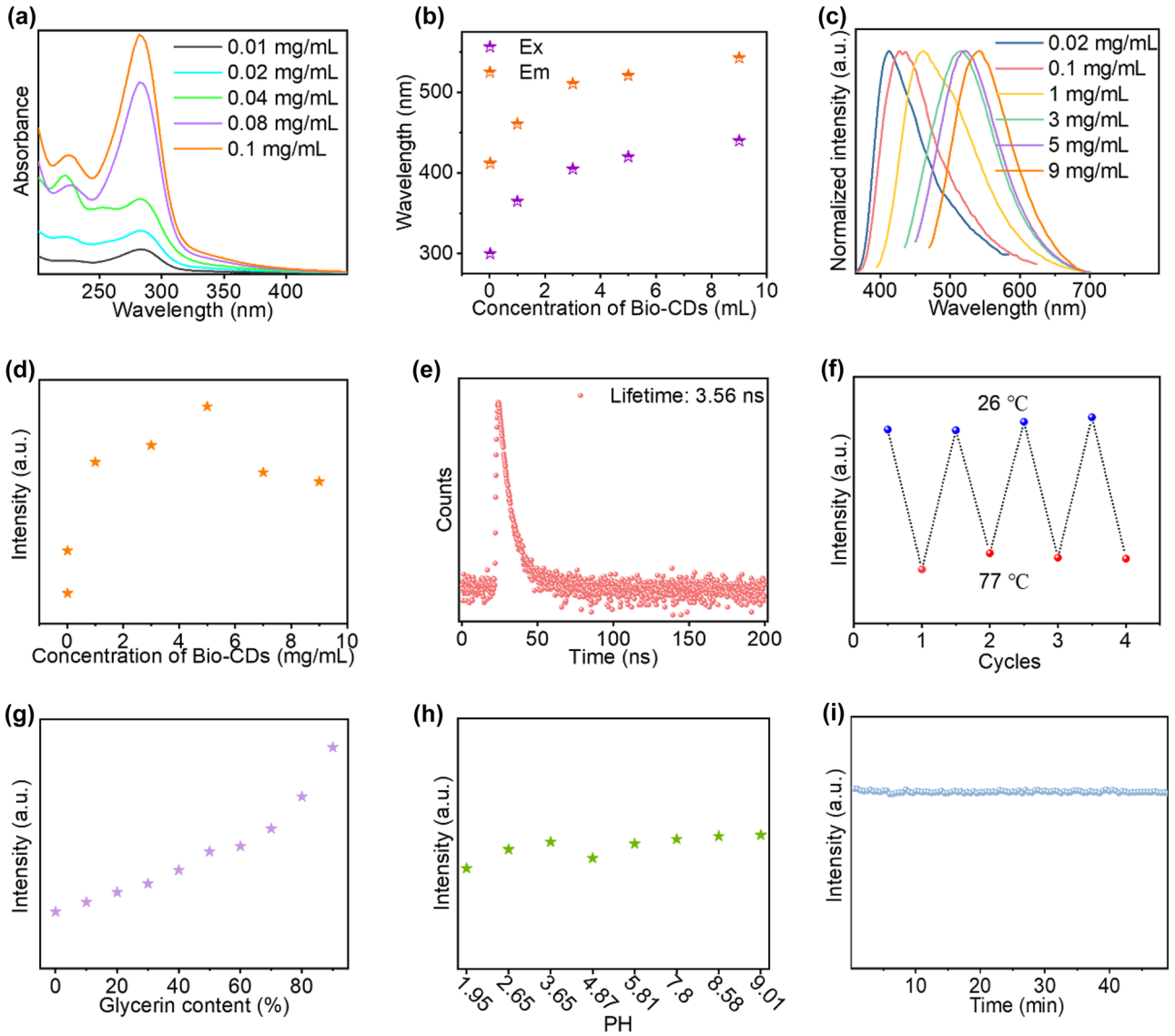

Fig. 3 **a** UV–Vis absorption spectra of Bio-CDs aqueous solutions with different concentrations (0.01–0.1 mg/mL); **b** fluorescence excitation and emission intensities of Bio-CDs aqueous solutions with different concentrations (0.02–9 mg/mL); **c** normalized intensity spectra of Bio-CDs aqueous solutions with different concentrations (0.02–9 mg/mL, Ex = 365 nm); **d** emission intensities of Bio-CDs aqueous solutions with different concentrations (0.02–9 mg/mL) at optimum excitation wavelength; **e** fluorescence decay curves of Bio-CDs aqueous solution (0.02 mg/mL); **f** fluorescence intensity of Bio-CDs aqueous solution (0.02 mg/mL) on repeated cycling between 26 and 77 °C; **g** fluorescence intensities of Bio-CDs aqueous solution (0.02 mg/mL) containing 0–90% glycerin; **h** fluorescence intensities of Bio-CDs aqueous solution (0.02 mg/mL) at different pH values; **i** fluorescence intensity of Bio-CDs aqueous solution (0.02 mg/mL) after continuous excitation at 365 nm for 50 min

optimal excitation wavelength redshifted from 300 to 440 nm (Fig. 3b) and the corresponding maximum emission wavelength redshifted from 411 to 541 nm as the concentration of Bio-CDs solution was increased (Fig. 3c); meanwhile, the CIE coordinates showed consistent color changes (Fig. S4). This is due to the increases of concentration, the Bio-CDs monomer aggregation leading to enhanced absorption and extends to longer wavelengths (Fig. 3a), which promotes n-π^* electron transition, thus causes long wavelength fluorescence emission [44, 45]. The above results showed that the optimal excitation and maximum emission wavelengths of Bio-CDs solution can be tuned by varying the concentration, that is, Bio-CDs has concentration-dependent long wavelength emission performance. Meanwhile, it confirmed the ability of Bio-CDs solution to absorb short wavelength light and convert it into long wavelength emission enhance with increasing concentration. Moreover, the emission intensity under optimal excitation first increases and then decreases as the concentration increases (Fig. 3d). This is explained by the fact that at low concentrations fluorescence enhancement

could be caused by the effect of increased concentration. At high concentrations (> 5 mg/mL), enhanced π-π interactions between carbon core leads to aggregation-caused quenching (ACQ) and a consequent reduction in emission intensity. In addition, re-absorption and excitation-dependence may also be reasons for the red shift and the emission intensity reduction [46]. The photoluminescence quantum yield (PLQY) of Bio-CDs aqueous solution was 6.3%, and the fluorescence lifetime was 3.56 ns. The decay curves of Bio-CDs solutions can be fitted to a double-exponential function (Fig. 3e, Table S1), indicating the presence of two fluorescence emitters, namely the carbon cores and surface fluorophores. Therefore, the luminescence mechanism of Bio-CDs solution is proposed: at low concentration, the carbon core state dominates the blue fluorescence emission, while at higher concentration, the surface state dominates the long wavelength fluorescence emission [17, 44].

To determine their practical utility, we also studied the effects of temperature, viscosity, and pH on the fluorescence emission intensity of the Bio-CDs. The emission intensity of the Bio-CDs gradually decreased with increasing temperature (Fig. S5). This temperature-induced photoluminescence quenching is thought to be closely associated with enhanced nonradiative relaxation [47, 48]. Reversible fluorescence emission was observed during several heating and cooling cycles (Fig. 3f). This good thermal cycling stability indicates that Bio-CDs can convert short wavelength light to long wavelength light emission at high temperatures. Glycerin was used to adjust the viscosity of the Bio-CDs solutions. The intensity of the fluorescence emission of the Bio-CDs in solution increased as the proportion of glycerin was increased (Figs. 3g and S6), consistent with previous reports on the nature of CDs [17, 25]. Changes in pH had little effect on the fluorescence emission intensity of Bio-CDs solutions (Figs. 3h and S7). When continuously excited with 365 nm UV light for 50 min, the emission intensity of an aqueous solution of Bio-CDs barely changed (Fig. 3i), demonstrating that the Bio-CDs have good resistance to photobleaching. These results confirm that the lack of sensitivity of the emission intensity of the Bio-CDs to pH, and that emission intensity of Bio-CDs solutions can be adjusted by changing the temperature and viscosity, while maintaining the ability to absorb short wavelength light and convert this into long wavelength emission. It is further shown that Bio-CDs can be used to block short wavelength photodamage in practical applications.

The Bio-CDs with good optical properties can be used for ink-jet printing and ion detection. First, an aqueous solution of Bio-CDs was used as a fluorescent ink to print different images. These images are colorless in natural light and produce blue fluorescence under 365 nm irradiation (Fig. S8). Next, we investigated the effects of different ions on the fluorescence intensity of aqueous solutions of Bio-CDs. Different anions (Fig. S9a) and most cations (Fig. S9b) had no effect on the fluorescence of the Bio-CDs. On the other hand, Fe^{3+} ions showed selective, concentration-dependent fluorescence quenching (Fig. S9c), with essentially complete quenching at an Fe^{3+} concentration of 1280 μM (Fig. S9d). Fluorescence quenching occurs because hydroxyl groups on the surface of the Bio-CDs form complexes with Fe^{3+}, leading to transfer of electrons from the Bio-CDs to the d orbitals of Fe^{3+} [49], thereby reducing the radiative transitions and inhibiting exciton recombination. The limit of detection (LOD) was 6.83 μM (Fig. S9d). The above results show that the Bio-CDs can be used as a fluorescent ink and for detection of Fe^{3+} ions.

The concentration-dependent long wavelength emission properties of the Bio-CDs aqueous solutions were well suited for applications field in blocking UV and blue light. The Bio-CDs were mixed with PVA to prepare optical shielding films (OSFs) with blocking UV and high-energy blue photons, which changed from colorless to brown with increasing concentrations of Bio-CDs (Fig. S10). Compared with pure PVA film, the OSFs had no effect on the visibility of the word "cellulose," indicating good transparency (Fig. S10). Enlarged cross-sectional SEM images of the OSFs showed that the Bio-CDs were uniformly dispersed in the PVA, and that the morphology of OSFs containing different proportions of Bio-CDs was similar (Fig. S11). The transmittance of pure PVA film in the blue-to-visible region (> 450 nm) is about 90% (Fig. 4a). As the proportion of Bio-CDs in the OSF increased, the transmittance at 200–450 nm gradually decreased (Fig. 4a), this was due to the increase of Bio-CDs content, which promotes the absorption for short wavelength light and thus reduced the transmittance (Fig. 3a), indicating that the OSFs strongly block both UV and high-energy blue photons. The emission of the OSFs is excitation wavelength-dependent (Fig. 4b) because of the presence of the Bio-CDs. After continuous excitation at 365 nm for 50 min, the emission intensity of the OSF was basically unchanged, showing good stability against photobleaching (Fig. 4c). As the proportion of Bio-CDs in the OSF was increased, the fluorescence emission spectra under excitation at 365 nm, 405 nm, and 450 nm showed that the OSFs can convert UV and high-energy blue light into harmless green-to-red light emission (Fig. S12), consistent with the CIE (1931) color coordinates (Fig. 4d–f). These results demonstrate that OSFs can absorb short wavelength light and convert it into long wavelength light, in the same way as Bio-CDs aqueous solutions.

The ability of the OSFs to block UV and blue light was investigated next using 395 and 450 nm LEDs. The extent of blocking of both 395 and 450 nm light increased as the proportion of Bio-CDs in the film increased and OSF containing 20% Bio-CDs completely blocked both 395 and 450 nm light (Figs. 4g–h and S13). OSFs thus have potential applications in blocking UV and blue light and the extent of blocking can be varied by adjusting content of Bio-CDs in the film. The

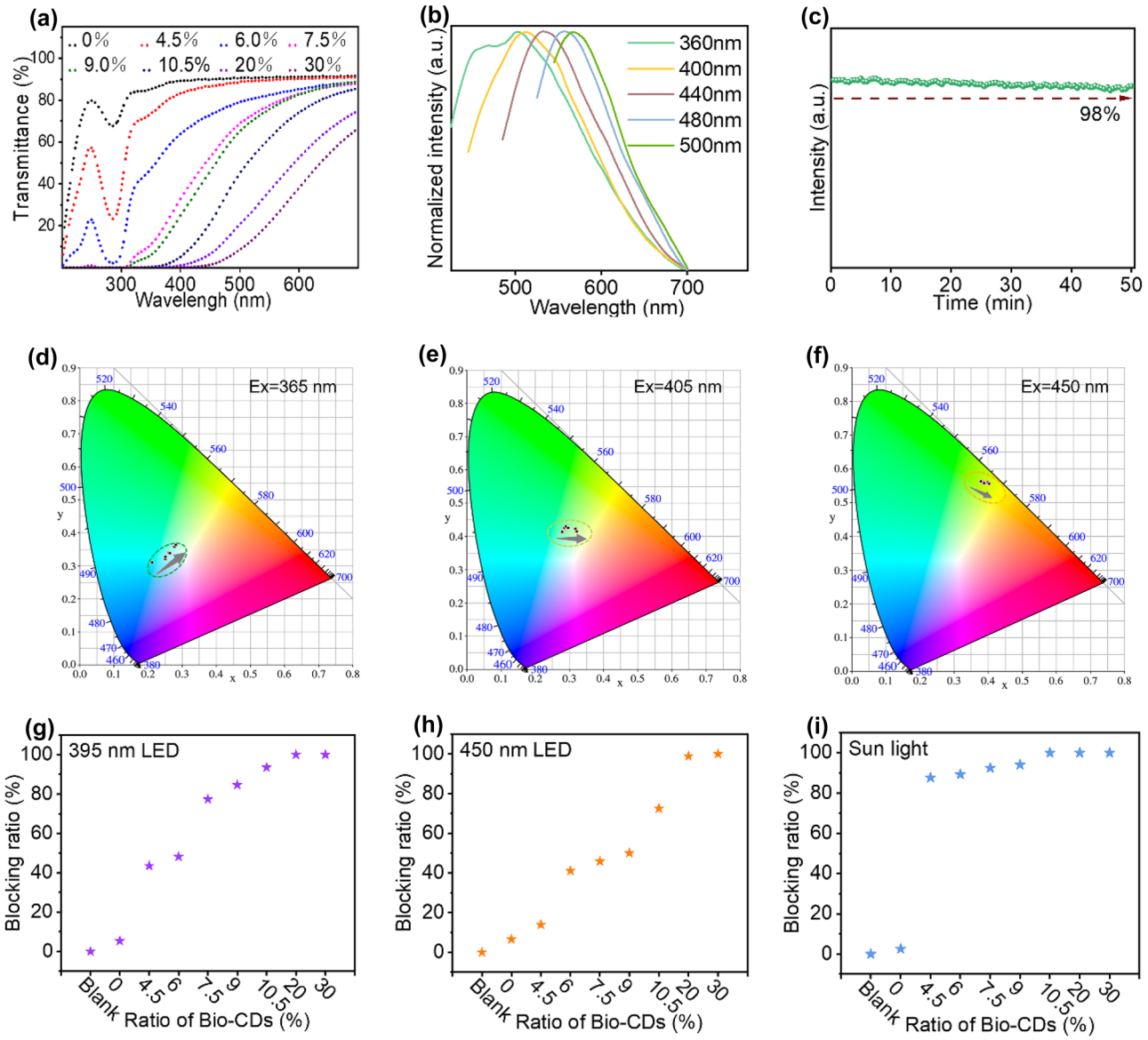

Fig. 4 **a** Transmittance of OSFs containing different proportions of Bio-CDs (0–30%); **b** normalized fluorescence emission spectra of OSF (10.5% Bio-CDs) at different excitation wavelengths; **c** fluorescence intensity of OSF (10.5% Bio-CDs) during continuous excitation at 365 nm for 50 min; **d**, **e**, **f** CIE (1931) coordinates diagram of OSFs (4.5–30% Bio-CDs) under different wavelength excitation at 365 nm, 405 nm, and 450 nm; **g**, **h**, **i** extent of blocking of UV (395 nm) light, blue (450 nm) light, and sun light by OSFs containing different proportions of Bio-CDs (0–30%)

ability of pure PVA and different OSFs to block UV radiation (≤400 nm) from the sun was also tested. As the proportion of Bio-CDs in the film was increased, the ability of the film to block solar UV light became greater and greater. When the proportion of CDs reached 10.5%, 100% of solar UV radiation was blocked (Figs. 4i and S14). The ability of OSFs to block UV rays from the sun was further investigated using commercially available UV test cards. Pure PVA film did not block UV light whereas OSFs very noticeably blocked UV radiation (Video S1). As the proportion of Bio-CDs in the OSFs was increased, the OSFs had better and better ability to block solar UV light. OSFs containing higher proportions of Bio-CDs provided a complete block.

As a practical application, we investigated the ability of OSFs to protect wood from discoloration damage caused by UV exposure, using white maple, basswood and balsa wood for the experiments (Fig. 5a–c, top). Sections of each wood were covered with OSFs (Fig. 5a–c, center) and the wood samples were then irradiated with intense UV light (340 nm, 80 W) for 90 h. Both uncovered woods and woods covered with pure PVA film became darker after UV irradiation (Fig. 5a–c bottom). The sections of the woods covered

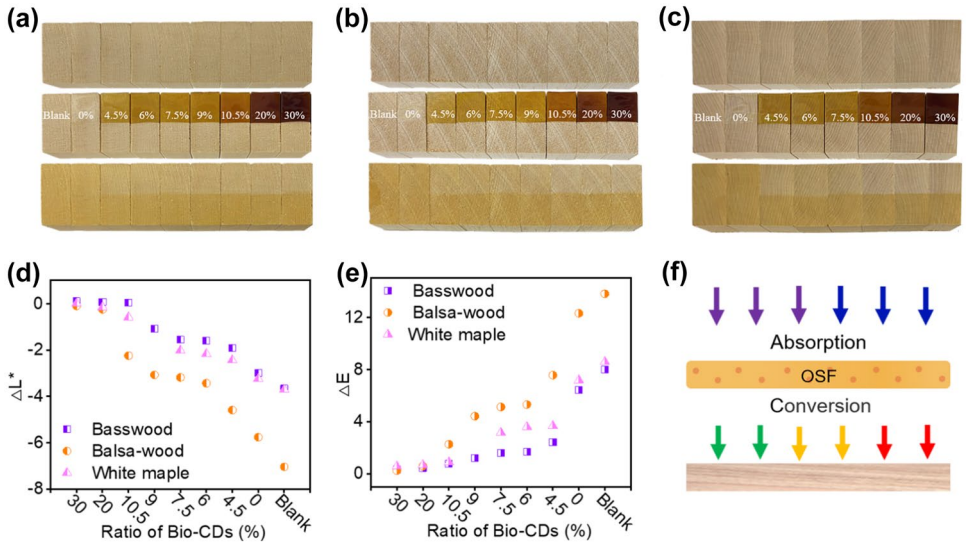

Fig. 5 **a** Photograph of initial basswood color (top), after coating with OSF (center) and after UV light irradiation (bottom); **b** photograph of initial balsa wood color (top), after coating with OSF (center) and after UV light irradiation (bottom); **c** photograph of initial white maple wood color (top), after coating with OSF (center), and after UV light irradiation (bottom); **d** curves showing changes in shade index value (ΔL^*) of OSF-coated woods after exposure to UV light; **e** curves showing changes in color difference value (ΔE) of OSF-coated woods after exposure to UV light; **f** schematic showing mechanism of blocking of UV/blue light by OSF

with the OSFs better retained their original color when the proportion of Bio-CDs in the OSF was higher because of the improved UV-blocking effect. These experiments demonstrate that the Bio-CDs contained in OSFs can effectively block the effect of UV rays on wood color. We next used a precision colorimeter to measure the changes in light and shade (ΔL^*) before and after exposure of the wood to UV light and calculated the color difference (ΔE) by formula (1). The greater the absolute value of ΔL^* and ΔE, the greater the change in color of the wood surface. The absolute value of ΔL^* and the ΔE value calculated after UV irradiation for the three woods covered with pure PVA film were the largest (Fig. 5d, e), that is, the surface color of the wood became darker. For wood samples covered with OSFs, the absolute value of ΔL^* and the ΔE value became smaller and smaller as the proportion of Bio-CDs in the OSF was increased (Fig. 5d, e), indicating a greater and greater degree of UV-blocking by the OSF. And OSF of 20% Bio-CDs can complete protect wood (Fig. 5d, e). This is because increased content of Bio-CDs in the OSF promote UV absorption and more efficient conversion of UV to longer wavelength light, thereby protecting the wood from UV damage. The effect of solar irradiation on the surface color of the wood was investigated by irradiating bare wood and wood with an OSF coating for 120 h, using a xenon lamp to simulate standard sunlight (AM1.5, 100 mW/cm^2) (Fig. S15). The color of the wood covered with pure PVA film darkened after simulated solar irradiation whereas wood covered with OSFs retained its original color. This is because, as the proportion of Bio-CDs in the film is increased, the OSF eventually absorbs all UV and high-energy blue photons and converts them into longer wavelength light emission [30], which then irradiates the surface of the wood, thus the direct exposure of UV light to the wood is avoided (Fig. 5f). These results clearly demonstrate that the newly developed OSFs can protect wood from damage caused by UV irradiation. A comparison of 20% OSF with other reported UV-blocking materials, in terms of environmental friendliness of raw materials, process simplicity, transparency, and sustainability, shows that 20% OSF has many advantages (Fig. 6 and Table S2). Therefore, the Bio-CDs are expected to find numerous practical applications in situations where it is desirable to protect materials from UV and high-energy blue light.

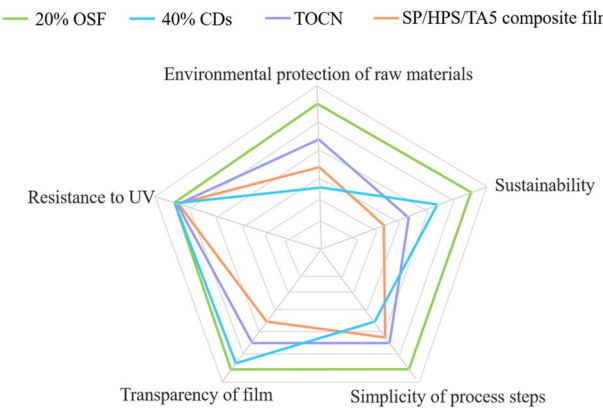

Fig. 6 Comparison of 20% OSF with other UV-blocking materials in terms of environmental friendliness of raw materials, process simplicity, transparency and sustainability

4 Conclusions

In summary, Bio-CDs with concentration-dependent emission were prepared using a one-step hydrothermal method, with microcrystalline cellulose as the raw material. OSFs, which could effectively block UV and high-energy blue photons, then were prepared by mixing the Bio-CDs with PVA. The blocking performance of the OSFs was studied using 395 nm and 450 nm LEDs as violet and blue light sources, respectively. As the proportion of Bio-CDs in the OSF was increased, the blocking of 395 and 450 nm light gradually increased until a complete barrier was formed. The OSF containing 10.5% Bio-CDs can completely blocked solar UV radiation ($\lesssim$400 nm). Our results demonstrate that the OSFs can block UV and high-energy blue photons and that the extent of blocking can be adjusted by varying the proportion of Bio-CDs in the OSF. The ability of OSFs containing different proportions of Bio-CDs to protect basswood, balsa wood, and white maple from UV-induced color changes was then investigated. Wood samples were coated with PVA film or OSFs and then irradiated with 340 nm UV light for 90 h. The surface color of uncoated wood and wood coated with pure PVA film became significantly darker. Wood coated with OSFs darkened to a lesser extent, and the protective effect increased gradually as the proportion of Bio-CDs in the film was increased. Wood coated with OSF containing 20% Bio-CDs can completed retain its original color. The same results were observed when the wood samples were irradiated with sunlight. OSF containing Bio-CDs can thus be used as an effective optical barrier material to protect wood from UV damage. This study implies that other CDs with concentration-dependent tunable emission can also be used as optical shielding units and are widely used in materials for blocking UV and high-energy blue photons.

Supplementary Information The online version contains supplementary material available at https://doi.org/10.1007/s42114-022-00619-8.

Author contribution The first two authors contributed equally to this work. Shiyan Han and Wenji Yu designed the research. Youqi Han carried out the experiments, data analysis, and drawing of figures. Yuning Wang, Yibing Bai, and Bin Zhao sorted the data and figures. Shujun Li and Chuanling Si carried out mechanism analysis. Zhijun Chen, Yahui Zhang, Haipeng Yu, and Chunlei Zhang carried out supervision. Youqi Han wrote the manuscript. All authors have given approval to the final version of the manuscript.

Funding This study was funded by the National Key Research and Development Program (2021YFD2200601).

Data availability All relevant data are within the paper and its Supporting Information files.

Declarations

Conflict of interest The authors declare no competing interests.

References

1. Palander T, Haavikko H, Kärhä K (2018) Towards sustainable wood procurement in forest industry-the energy efficiency of larger and heavier vehicles in Finland. Renew Sust Energ Rev 96:100–118. https://doi.org/10.1016/j.rser.2018.07.043
2. Voshell S, Mäkelä M, Dahl O (2018) A review of biomass ash properties towards treatment and recycling. Renew Sust Energ Rev 96:479–486. https://doi.org/10.1016/j.rser.2018.07.025
3. Head M, Bernier P, Levasseur A, Beauregard R, Margni M (2019) Forestry carbon budget models to improve biogenic carbon accounting in life cycle assessment. J Clean Prod 213:289–299. https://doi.org/10.1016/j.jclepro.2018.12.122
4. Wang J, Zhang D, Chu F (2021) Wood-derived functional polymeric materials. Adv Mater 33:e2001135. https://doi.org/10.1002/adma.202001135
5. Mi R, Chen C, Keplinger T, Pei Y, He S, Liu D, Li J, Dai J, Hitz E, Yang B, Burgert I, Hu L (2020) Scalable aesthetic transparent wood for energy efficient buildings. Nat Commun 11:3836. https://doi.org/10.1038/s41467-020-17513-w
6. Jia C, Chen C, Mi R, Li T, Dai J, Yang Z, Pei Y, He S, Bian H, Jang S, Zhu J, Yang B, Hu L (2019) Clear wood toward high-performance building materials. ACS Nano 13:9993–10001. https://doi.org/10.1021/acsnano.9b00089
7. Li W, Chen Z, Yu H, Li J, Liu S (2021) Wood-derived carbon materials and light-emitting materials. Adv Mater 33:e2000596. https://doi.org/10.1002/adma.202000596
8. Guo H, Klose D, Hou Y, Jeschke G, Burgert I (2017) Highly efficient UV protection of the biomaterial wood by a transparent TiO_2/Ce xerogel. ACS Appl Mater Interfaces 9:39040–39047. https://doi.org/10.1021/acsami.7b12574
9. Xia Q, Chen C, Yao Y, He S, Wang X, Li J, Gao J, Gan W, Jiang B, Cui M, Hu L (2021) In situ lignin modification toward photonic wood. Adv Mater 33:e2001588. https://doi.org/10.1002/adma.202001588
10. Yang H, Liu Y, Guo Z, Lei B, Zhuang J, Zhang X, Liu Z, Hu C (2019) Hydrophobic carbon dots with blue dispersed emission and red aggregation-induced emission. Nat Commun 10:1789. https://doi.org/10.1038/s41467-019-09830-6
11. Varganici C, Rosu L, Rosu D, Mustata F, Rusu T (2020) Sustainable wood coatings made of epoxidized vegetable oils for ultraviolet protection. Environ Chem Lett 19:307–328. https://doi.org/10.1007/s10311-020-01067-w
12. Yuan B, Guo M, Murugadoss V, Song G, Guo Z (2021) Immobilization of graphitic carbon nitride on wood surface via chemical crosslinking method for UV resistance and self-cleaning. Adv Compos Hybrid Mater 4:286–293. https://doi.org/10.1007/s42114-021-00235-y
13. Dong Y, Yan Y, Ma H, Zhang S, Li J, Xia C, Shi S, Cai L (2017) In-situ chemosynthesis of ZnO nanoparticles to endow wood with antibacterial and UV-resistance properties. J Mater Sci Technol 33:266–270. https://doi.org/10.1016/j.jmst.2016.03.018
14. Lim S, Shen W, Gao Z (2015) Carbon quantum dots and their applications. Chem Soc Rev 44:362–381. https://doi.org/10.1039/c4cs00269e
15. Desmond L, Phan A, Gentile P (2021) Critical overview on the green synthesis of carbon quantum dots and their application for cancer therapy. Environ Sci-Nano 8:848–862. https://doi.org/10.1039/d1en00017a
16. Wareing T, Gentile P, Phan A (2021) Biomass-based carbon dots: current development and future perspectives. ACS Nano 15:15471–15501. https://doi.org/10.1021/acsnano.1c03886
17. Ge M, Han Y, Ni J, Li Y, Han S, Li S, Yu H, Zhang C, Liu S, Li J, Chen Z (2021) Seeking brightness from nature: sustainable carbon dots-based AIEgens with tunable emission wavelength from natural

rosin. Chem Eng J 413:127457. https://doi.org/10.1016/j.cej.2020.127457
18. Ge M, Huang X, Ni J, Han Y, Zhang C, Li S, Cao J, Li J, Chen Z, Han S (2021) One-step synthesis of self-quenching-resistant biomass-based solid-state fluorescent carbon dots with high yield for white lighting emitting diodes. Dyes Pigments 185:108953. https://doi.org/10.1016/j.dyepig.2020.108953
19. Cai X, Lin Y, Li Y, Chen X, Wang Z, Zhao X, Huang S, Zhao Z, Tang B (2021) BioAIEgens derived from rosin: how does molecular motion affect their photophysical processes in solid state? Nat Commun 12:1773. https://doi.org/10.1038/s41467-021-22061-y
20. Liu H, Du H, Zheng T, Liu K, Ji X, Xu T, Zhang X, Si C (2021) Cellulose based composite foams and aerogels for advanced energy storage devices. Chem Eng J. https://doi.org/10.1016/j.cej.2021.130817
21. Liu H, Xu T, Cai C, Liu K, Liu W, Zhang M, Du H, Si C, Zhang K (2022) Multifunctional superelastic, superhydrophilic, and ultralight nanocellulose-based composite carbon aerogels for compressive supercapacitor and strain sensor. Adv Funct Mater. https://doi.org/10.1002/adfm.202113082
22. Xu T, Du H, Liu H, Liu W, Zhang X, Si C, Liu P, Zhang K (2021) Advanced nanocellulose-based composites for flexible functional energy storage devices. Adv Mater 33:e2101368. https://doi.org/10.1002/adma.202101368
23. Zhang M, Du H, Liu K, Nie S, Xu T, Zhang X, Si C (2021) Fabrication and applications of cellulose-based nanogenerators. Adv Compos Hybrid Mater 4:865–884. https://doi.org/10.1007/s42114-021-00312-2
24. Xu T, Liu K, Sheng N, Zhang M, Liu W, Liu H, Dai L, Zhang X, Si C, Du H, Zhang K (2022) Biopolymer-based hydrogel electrolytes for advanced energy storage/conversion devices: properties, applications, and perspectives. Energy Storage Mater 48:244–262. https://doi.org/10.1016/j.ensm.2022.03.013
25. Han Y, Huang X, Liu J, Ni J, Bai Y, Zhao B, Han S, Zhang C (2022) Seeking eye protection from biomass: carbon dot-based optical blocking films with adjustable levels of blue light blocking. J Colloid Interf Sci 617:44–52. https://doi.org/10.1016/j.jcis.2022.02.115
26. Park S, Yang H, Moon B (2019) Ultraviolet to blue blocking and wavelength convertible films using carbon dots for interrupting eye damage caused by general lighting. Nano Energy 60:87–94. https://doi.org/10.1016/j.nanoen.2019.03.043
27. Wang R, Meng Z, Yan X, Tian T, Lei M, Pashameah R, Abo-Dief H, Algadi H, Huang N, Guo Z, Tang H (2023) Tellurium intervened Fe-N codoped carbon for improved oxygen reduction reaction and high-performance Zn-air batteries. J Mater Sci Technol 137:215–222. https://doi.org/10.1016/j.jmst.2022.07.041
28. Liu S, Du H, Liu K, Ma M, Kwon Y, Si C, Ji X, Choi S, Zhang X (2021) Flexible and porous Co3O4-carbon nanofibers as binder-free electrodes for supercapacitors. Adv Compos Hybrid Mater 4:1367–1383. https://doi.org/10.1007/s42114-021-00344-8
29. Chen N, Wang C, Ali O, Mahmoud S, Shi Y, Ji Y, Algadi H, EI-Bahy S, Huang M, Guo Z, Cui D, Wei H (2022) MXene@nitrogen-doped carbon films for supercapacitor and piezoresistive sensing applications. Compos A 163:107174. https://doi.org/10.1016/j.compositesa.2022.107174
30. Hou C, Yang W, Kimura H, Xie X, Zhang X, Sun X, Yu Z, Yang X, Zhang Y, Wang B, Xu B, Sridhar D, Algadi H, Guo Z, Du W (2023) Boosted lithium storage performance by local build-in electric field derived by oxygen vacancies in 3D holey N-doped carbon structure decorated with molybdenum dioxide. J Mater Sci Technol 142:185–195. https://doi.org/10.1016/j.jmst.2022.10.007
31. Xue B, Yang Y, Sun Y, Fan J, Li X, Zhang Z (2019) Photoluminescent lignin hybridized carbon quantum dots composites for bioimaging applications. Int J Biol Macromol 122:954–961. https://doi.org/10.1016/j.ijbiomac.2018.11.018
32. Ozyurt D, Shafqat S, Pakkanen T, Hocking R, Mouritz A, Fox B (2021) Aggregation induced emission transformation of liquid and solid-state N-doped graphene quantum dots. Carbon 175:576–584. https://doi.org/10.1016/j.carbon.2021.01.026
33. Liu H, Xu T, Liang Q, Zhao Q, Zhao D, Si C (2022) Compressible cellulose nanofibrils/reduced graphene oxide composite carbon aerogel for solid-state supercapacitor. Adv Compos Hybrid Mater 5:1168–1179. https://doi.org/10.1007/s42114-022-00427-0
34. Wang Z, Liu Y, Zhen S, Li X, Zhang W, Sun X, Xu B, Wang X, Gao Z, Meng X (2020) Gram-scale synthesis of 41% efficient single-component white-light-emissive carbonized polymer dots with hybrid fluorescence/phosphorescence for white Light-Emitting Diodes. Adv Sci 7:1902688. https://doi.org/10.1002/advs.201902688
35. Zeng M, Li T, Liu Y, Lin X, Zu X, Mu Y, Chen L, Huo Y, Qin Y (2022) Cellulose-based photo-enhanced persistent room-temperature phosphorescent materials by space stacking effects. Chem Eng J. https://doi.org/10.1016/j.cej.2022.136935
36. Xu M, Dong C, Xu J, Rehman S, Wang Q, Osipov V, Jiang K, Wang J, Bi H (2022) Fluorinated carbon dots/carboxyl methyl cellulose sodium composite with a temperature-sensitive fluorescence/phosphorescence applicable for anti-counterfeiting marking. Carbon 189:459–466. https://doi.org/10.1016/j.carbon.2021.12.077
37. Chen W, Hong L, Wu Y, Yang M, Zhang X, Zhu S, He M, Xie J, Shi Z (2022) Fluorescent probe of nitrogen-doped carbon dots derived from biomass for the sensing of MnO4-in polluted water based on inner filter effect. Adv Compos Hybrid Mater 5:2378–2386. https://doi.org/10.1007/s42114-022-00443-0
38. Vijeata A, Chaudhary G, Umar A, Chaudhary S (2021) Distinctive solvatochromic response of fluorescent carbon dots derived from different components of aegle marmelos plant. Eng Sci 15:197–209. https://doi.org/10.30919/es8e512
39. Liu B, Chu B, Wang Y, Hu L, Hu S, Zhang X (2021) Carbon dioxide derived carbonized polymer dots for multicolor light-emitting diodes. Green Chem 23:422–429. https://doi.org/10.1039/d0gc03333b
40. Jiang K, Gao X, Feng X, Wang Y, Li Z, Lin H (2020) Carbon dots with dual-emissive, robust, and aggregation-induced room-temperature phosphorescence characteristics. Angew Chem Int Ed Engl 59:1263–1269. https://doi.org/10.1002/anie.201911342
41. Han Y, Tang B, Wang L, Bao H, Lu Y, Guan C, Zhang L, Le M, Liu Z, Wu M (2020) Machine-learning-driven synthesis of carbon dots with enhanced quantum yields. ACS Nano 14:14761–14768. https://doi.org/10.1021/acsnano.0c01899
42. Guo J, Li H, Ling L, Li G, Cheng R, Lu X, Xie A, Li Q, Wang C, Chen S (2019) Green synthesis of carbon dots toward anti-counterfeiting. ACS Sustain Chem Eng 8:1566–1572. https://doi.org/10.1021/acssuschemeng.9b06267
43. Kumari M, Chaudhary G, Chaudhary S, Umar A (2022) Rapid analysis of trace sulphite ion using fluorescent carbon dots produced from single use plastic cups. Eng Sci 17:101–112. https://doi.org/10.30919/es8d556
44. Ba X, Zhang L, Yin Y, Jiang F, Jiang P, Liu Y (2020) Luminescent carbon dots with concentration-dependent emission in solution and yellow emission in solid state. J Colloid Interface Sci 565:77–85. https://doi.org/10.1016/j.jcis.2020.01.007
45. Ni J, Huang X, Bai Y, Zhao B, Han Y, Han S, Xu T, Si C, Zhang C (2022) Resistance to aggregation-caused quenching: chitosan-based solid carbon dots for white light-emitting diode and 3D printing. Adv Compos Hybrid Mater 5:1865–1875. https://doi.org/10.1007/s42114-022-00483-6
46. Chen Y, Zheng M, Xiao Y, Dong H, Zhang H, Zhuang J, Hu H, Lei B, Liu Y (2016) A Self-quenching-resistant carbon-dot powder with tunable solid-state fluorescence and construction of dual-fluorescence morphologies for white light-emission. Adv Mater 28:312–318. https://doi.org/10.1002/adma.201503380

47. Bhattacharyya S, Ehrat F, Urban P, Teves R, Wyrwich R, Doblinger M, Feldmann J, Urban A, Stolarczyk J (2017) Effect of nitrogen atom positioning on the trade-off between emissive and photocatalytic properties of carbon dots. Nat Commun 8:1401. https://doi.org/10.1038/s41467-017-01463-x
48. Zhang T, Zhao F, Li L, Qi B, Zhu D, Lu J, Lu C (2018) Tricolor White-light-emitting carbon dots with multiple-cores@shell structure for WLED application. ACS Appl Mater Interfaces 10:19796–19805. https://doi.org/10.1021/acsami.8b03529
49. Gao X, Zhou X, Ma Y, Qian T, Wang C, Chu F (2019) Facile and cost-effective preparation of carbon quantum dots for Fe^{3+} ion and ascorbic acid detection in living cells based on the "on-off-on" fluorescence principle. Appl Surf Sci 469:911–916. https://doi.org/10.1016/j.apsusc.2018.11.095